Continuous N_2O capture and reduction to N_2 using Ca-zeolite adsorbent and $Pd/La/Al_2O_3$ reduction catalyst

Yuan Jing,*[†] Chenxi He,[†] Li Wan,[†] Jiahuan Tong,[†] Jialei Zhang,[†] Shinya Mine,[⊥] Ningqiang Zhang,[†] Yuuta Kageyama,[‡] Hironori Inomata,[‡] Ken-ichi Shimizu*[,†], Takashi Toyao*[,†]

[†] Institute for Catalysis, Hokkaido University, N-21, W-10, Sapporo 001-0021, Japan

[⊥] Research Institute for Chemical Process Technology, National Institute of Advanced Industrial Science and Technology (AIST), 4-2-1, Nigatake, Miyagino-ku, Sendai 983-8551, Japan

[‡] Isuzu Motors, Ltd., 8 Tsuchidana, Fujisawa 252-0881, Japan

Abstract

There is an urgent need to develop effective methods for converting nitrous oxide (N_2O) into non-harmful N_2 because N_2O is a potent greenhouse gas, and its increasing concentration in the atmosphere is a major concern for global warming. In this study, we developed a two-step N_2O capture and reduction system, employing CaO-incorporated zeolites (Ca-zeolites) as N_2O adsorbents and Pd nanoparticles on La-containing Al_2O_3 ($Pd/La/Al_2O_3$) as catalysts for N_2O reduction. This process is suitable for continuous operation over a temperature swing of 50–150 °C. The N_2O capture capacity and subsequent reduction ability were preserved for at least 15 h (10 cycles). Notably, this system can operate at low temperatures (below 150 °C) using a simple temperature-swing process in the presence of O_2.

https://doi.org/10.26434/chemrxiv-2024-0q1cm **ORCID:** https://orcid.org/0000-0002-6100-8247 Content not peer-reviewed by ChemRxiv. **License:** CC BY-NC 4.0

Introduction

It is well known that N_2O has a global warming potential approximately 300 times greater than that of CO_2 on a per-mass basis. Additionally, N_2O is a significant contributor to stratospheric ozone depletion.[1–3] Emissions of N_2O from industries that use fossil fuels, burn biomass, and chemical plants that produce nitric and adipic acids are increasing annually.[4] Without global mitigation efforts, N_2O emissions are expected to nearly double by 2050.[5] Consequently, effective catalytic post-treatment technologies must be developed to treat the N_2O emissions from stationary systems and vehicles burning transportation fuels.

Various methods exist for decomposing N_2O into harmless N_2, such as thermal, electrocatalytic, and photocatalytic systems.[6–12] Although electrocatalytic and photocatalytic systems can operate at ambient temperatures, their catalytic activities are reduced in the presence of O_2. Processes based on thermal catalysis can decompose N_2O even in the presence of O_2 through direct decomposition ($2N_2O = 2N_2 + O_2$)[13–21] or selective catalytic reduction[22–28] methods but both of these require high temperatures, typically above 300 °C. Therefore, it is essential to devise methods that can efficiently decompose N_2O even in the presence of O_2, especially at low temperatures.

In recent years, chemical looping has been increasingly recognized as an effective technique for various chemical transformations, particularly those associated with CO_2 utilization.[29,30] For instance, a chemical-looping system for CO_2 utilization employs CO_2 adsorbents and CO_2 reduction materials that can operate in various reactors.[31–33] This process can be used for CO_2 transformation in the presence of O_2 because the chemical absorption of CO_2 is not inhibited by O_2, and H_2 as a reductant is not simultaneously introduced into the same reactor as O_2. This is advantageous from a practical viewpoint because O_2 is often present in waste gases containing CO_2.

In this study, inspired by the aforementioned chemical-looping strategy, we developed an N_2O capture and reduction system that uses CaO-incorporated zeolites (Ca-zeolites) as N_2O adsorbents and Pd nanoparticles on La-containing Al_2O_3 (Pd/La/Al_2O_3) as the reduction catalyst. This new process is suitable for continuous operation under temperature-swing cycling between 50 and 150 °C. The N_2O capture capacity and subsequent reduction ability were maintained for at least 15 h (10 cycles). Notably, this process can be performed at low temperatures (below 150 °C) via a simple temperature-swing operation in the presence of O_2.

Results and discussion

Catalyst properties

Figure 1 shows the N_2O-TPD profiles of various ion-exchanged zeolite materials. The desorption amount of N_2O in the temperature range of 50–250 °C was used to compare the adsorption capacity of N_2O. The obtained results show that the ion-exchanged Ca-MOR zeolite exhibited the highest N_2O adsorption capacity at 50 °C compared with the other samples prepared in this study. In addition, Ca-

https://doi.org/10.26434/chemrxiv-2024-0q1cm **ORCID:** https://orcid.org/0000-0002-6100-8247 Content not peer-reviewed by ChemRxiv. **License:** CC BY-NC 4.0

$MOR_{Si/Al=110}$ and Ca-$MFI_{Si/Al=90}$, which were prepared by ion-exchange method using zeolites with high Si/Al ratios, exhibit negligible N_2O adsorption at 50 °C, indicating that the amount of Al sites in the zeolite plays an important role in N_2O adsorption. **Figure 2** shows X-ray diffraction (XRD) patterns of the Ca-exchanged MOR (Ca-MOR) and H-MOR samples. The XRD peaks observed for Ca-MOR are identical to those of H-MOR, without the presence of peaks for Ca species, indicating that the Ca species in Ca-MOR are well dispersed.

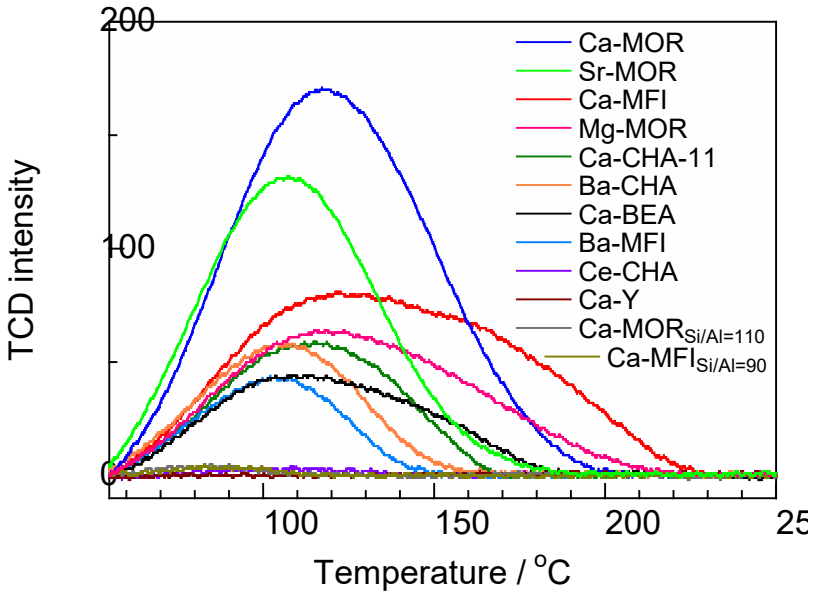

Figure 1. N_2O-TPD profile over different ion-exchanged zeolite materials after exposure to 10% N_2O/He at 50 °C for 30 min followed by a He purge for 10 min. The sample was heated from 50 to 250 °C at a rate of 10 °C/min.

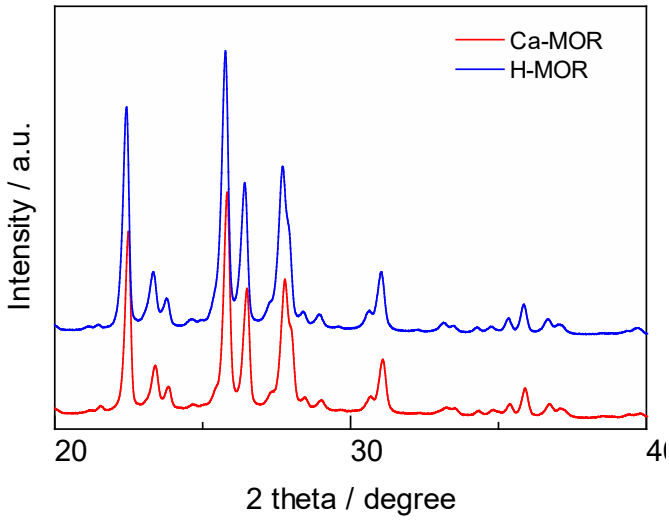

Figure 2. XRD patterns of H-MOR and Ca-MOR zeolites.

A computational investigation was conducted to clarify the possible structures of the CaO species introduced in the zeolite. An *ab initio* thermodynamic approach was used to evaluate the system stability under certain conditions by calculating the Gibbs free energy change (ΔG) values. Three types of MOR zeolites with different Al positions and sites were considered in this study: (i)

https://doi.org/10.26434/chemrxiv-2024-0q1cm **ORCID:** https://orcid.org/0000-0002-6100-8247 Content not peer-reviewed by ChemRxiv. **License:** CC BY-NC 4.0

MOR with one Al atom, (ii) MOR with two Al in an 8-membered ring (8MR), and (iii) MOR with two Al in a 5-membered ring (5MR), as shown in **Figure S1**.[34–37] The Al position in structure (VIII) is the most stable and widely used. We also investigated the position of the second Al atom by fixing the first atom and selecting structures (VII) and (II) as representative models with fairly stable structures to investigate the 5MR and 8MR as possible Al sites (**Figure S2**). Subsequently, various Ca oxide clusters with 1–3 Ca atoms were placed in each structure (**Figure S3–S5**). Only the most stable structures for each chemical formulation are depicted for clarity. The valence state of Ca was set to 2+ for all structures because other valence states, such as 0 and +1, are unlikely under ambient conditions. **Figure 3** shows the phase diagram of the Ca oxide species with the lowest Δ*G* values as a function of the temperature and partial pressure of O_2. The results were obtained using VASP. Only mononuclear and dinuclear Ca species were stable in all MOR models, whereas the trimeric species were relatively unstable under these conditions.

The same *ab initio* thermodynamic analysis was performed using the computational results calculated by Matlantis instead of Vienna Ab Initio Simulation Package (VASP)[38,39]. Matlantis employs universal neural network potentials called PreFerred Potentials, which support various elements and material types with an accuracy comparable to that of density-function theory (DFT) calculations and with significantly lower computational costs.[40] If rational results can be obtained with Matlantis, this would enable us to significantly reduce the computational time, even for unknown systems. **Figure S6** displays a phase diagram of the Ca species with the lowest Δ*G* values as a function of the temperature and partial pressure of O_2 obtained from the computational results calculated by Matlantis. These results are similar to those obtained using VASP, confirming the high reliability of Matlantis. The *ab initio* thermodynamic results indicate that mononuclear and dinuclear species can be produced under the investigated experimental conditions, which is consistent with the XRD results.

https://doi.org/10.26434/chemrxiv-2024-0q1cm **ORCID:** https://orcid.org/0000-0002-6100-8247 Content not peer-reviewed by ChemRxiv. **License:** CC BY-NC 4.0

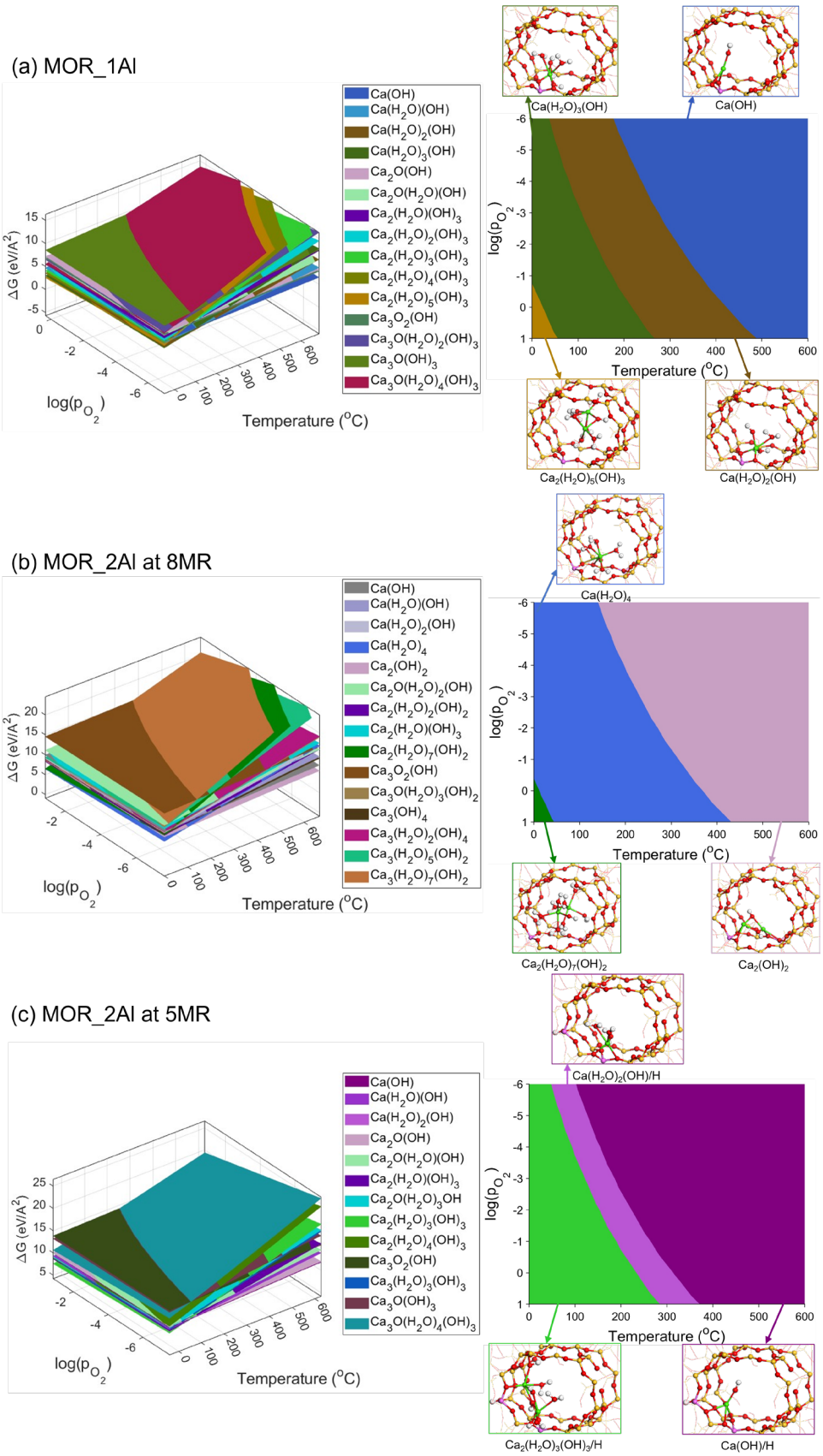

Figure 3. 3D (left) and 2D (right) phase diagrams for (a) MOR_1Al, (b) MOR_2Al at 8MR, and (c) MOR_2Al at 5MR showing the species with the lowest Gibbs free energy change (ΔG) in terms of temperature and O_2 partial pressure (log scale) and possible structures. All calculations were performed using VASP (green, Ca; pink, Al; red, O; yellow, Si; white, H).

https://doi.org/10.26434/chemrxiv-2024-0q1cm **ORCID:** https://orcid.org/0000-0002-6100-8247 Content not peer-reviewed by ChemRxiv. **License:** CC BY-NC 4.0

N_2O adsorption/desorption and breakthrough results

The *in situ* infrared (IR) spectra of N_2O adsorbed on Ca-MOR and H-MOR at 50 °C are shown in **Figure 4A**. No adsorption peaks were observed for H-MOR, indicating that no N_2O molecules were adsorbed onto its surface. After Ca-MOR was exposed to N_2O, two peaks at 2246 and 2273 cm^{-1} were observed, which are assigned to the N–N vibrational mode of N_2O molecules adsorbed on Ca sites.[41–43] These results indicate that the Ca species in Ca-MOR account for its superior N_2O adsorption capacity. **Figure 4A** also shows the *in situ* IR spectra of N_2O adsorbed on Ca-MOR collected under He with increasing temperature from 50 to 150 °C after exposure to 0.1% N_2O/He for 30 min and subsequent purging under He. The intensity of the N_2O molecules adsorbed on the Ca species decreased with increasing temperature, and gaseous N_2O was detected in the effluent of the *in situ* IR cell, as shown in **Figure 4B**. A desorption peak of N_2O was observed at ~90 °C with a shoulder peak at ~125 °C, suggesting the presence of adsorbed N_2O molecules with different adsorption strengths.

Under practical conditions, O_2, CO_2, and H_2O often coexist in N_2O feed gas.[44,45] Therefore, breakthrough experiments were performed to investigate the effects of O_2, CO_2, and H_2O on the adsorption capacity of N_2O of Ca-MOR. The results of the breakthrough experiments (**Figure 5**) show that the presence of O_2 has almost no impact on the N_2O capture ability of Ca-MOR, indicating that Ca-MOR can selectively capture N_2O in the presence of O_2. However, the presence of 3% H_2O decreased the adsorption amount of N_2O on Ca-MOR significantly. The Ca-MOR only exhibited limited N_2O adsorption capacity in the presence of 5% CO_2. These results indicate that CO_2 and H_2O should be removed from the N_2O feed to ensure that Ca-MOR maintains high efficiency for N_2O capture.

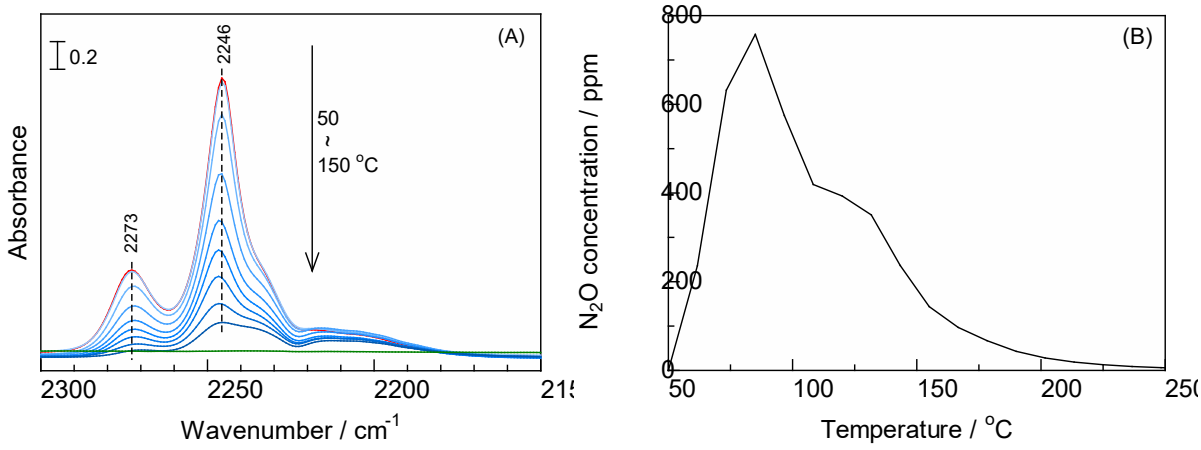

Figure 4. (A) *In situ* IR spectra of N_2O adsorbed on Ca-MOR under the flow of He; red/green: N_2O adsorbed on Ca-MOR/H-MOR at 50 °C after purging under He for 30 min followed by the introduction of 0.1% N_2O/He for 30 min; blue: N_2O adsorbed on Ca-MOR during heating from 50 to 150 °C. (B) Concentration of N_2O in the effluent of the *in situ* IR cell during the measurement with Ca-MOR while increasing the temperature of the *in situ* cell from 50 to 150 °C at a rate of 10 °C/min.

https://doi.org/10.26434/chemrxiv-2024-0q1cm **ORCID:** https://orcid.org/0000-0002-6100-8247 Content not peer-reviewed by ChemRxiv. **License:** CC BY-NC 4.0

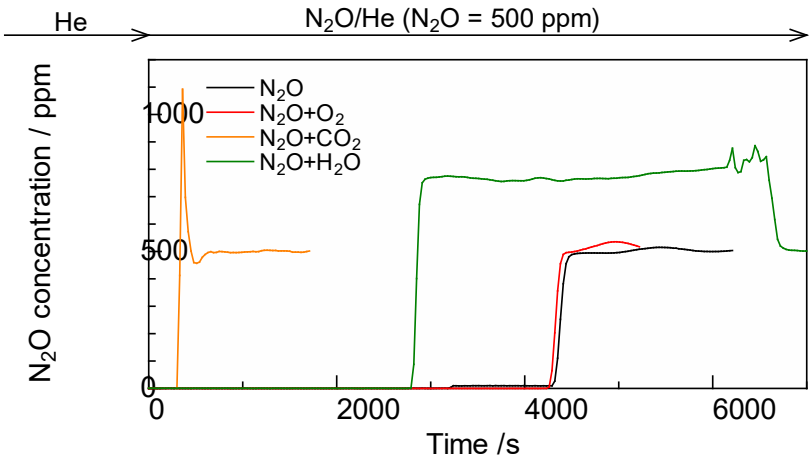

Figure 5. Profile of the breakthrough experiments over Ca-MOR zeolite under a flow of (a) 500 ppm N_2O, (b) 500 ppm N_2O + 10% O_2, (c) 500 ppm N_2O + 5% CO_2, and (d) 500 ppm N_2O + 3% H_2O at 50 °C. Weight of Ca-MOR: 100 mg, total flow rate = 50 mL/min, He balance.

Figure 6 shows the *in situ* IR spectra of N_2O adsorbed on Ca/MOR after the introduction of O_2, CO_2, or H_2O. The spectra of N_2O adsorbed on Ca-MOR were collected after the introduction of 0.1% N_2O at 50 °C for 30 min. After the introduction of 10% O_2 to the N_2O feed gas, the absorbance intensity of adsorbed N_2O exhibited almost no change, indicating that the presence of O_2 negligibly affects the adsorption of N_2O, which is consistent with the results of the breakthrough experiments. After the introduction of CO_2, the intensities of the peaks at 2273 and 2246 cm^{-1} decreased, and a new peak appeared at 1377 cm^{-1} (**Figure 6B**). The peak at 1377 cm^{-1} was assigned to CO_2 adsorbed on Ca species in zeolite.[46] The peaks related to the adsorption of N_2O onto Ca sites were not observed after the introduction of 5% CO_2 for 10 min. These results suggest that the presence of CO_2 inhibited the adsorption of N_2O because of the higher adsorption strength of CO_2 on Ca than that of N_2O. A similar evolution of the peaks of adsorbed N_2O was observed after the introduction of 3% H_2O (**Figure 6C**). After the introduction of 3% H_2O, the peak intensity of adsorbed N_2O decreased, and the peak at 1625 cm^{-1} related to adsorbed H_2O, increased.

We conducted a theoretical investigation of the adsorption energies of various adsorbates, such as N_2O, CO_2, H_2O, and O_2 on the Ca-oxo clusters in MOR zeolite, which were identified by ab initio thermodynamic analysis using VASP. Overall, we found that the adsorption of N_2O was weaker than that of CO_2 or H_2O but stronger than that of O_2 (**Figure S7**). These results are in good agreement with the findings of the *in situ* IR experiments.

https://doi.org/10.26434/chemrxiv-2024-0q1cm **ORCID:** https://orcid.org/0000-0002-6100-8247 Content not peer-reviewed by ChemRxiv. **License:** CC BY-NC 4.0

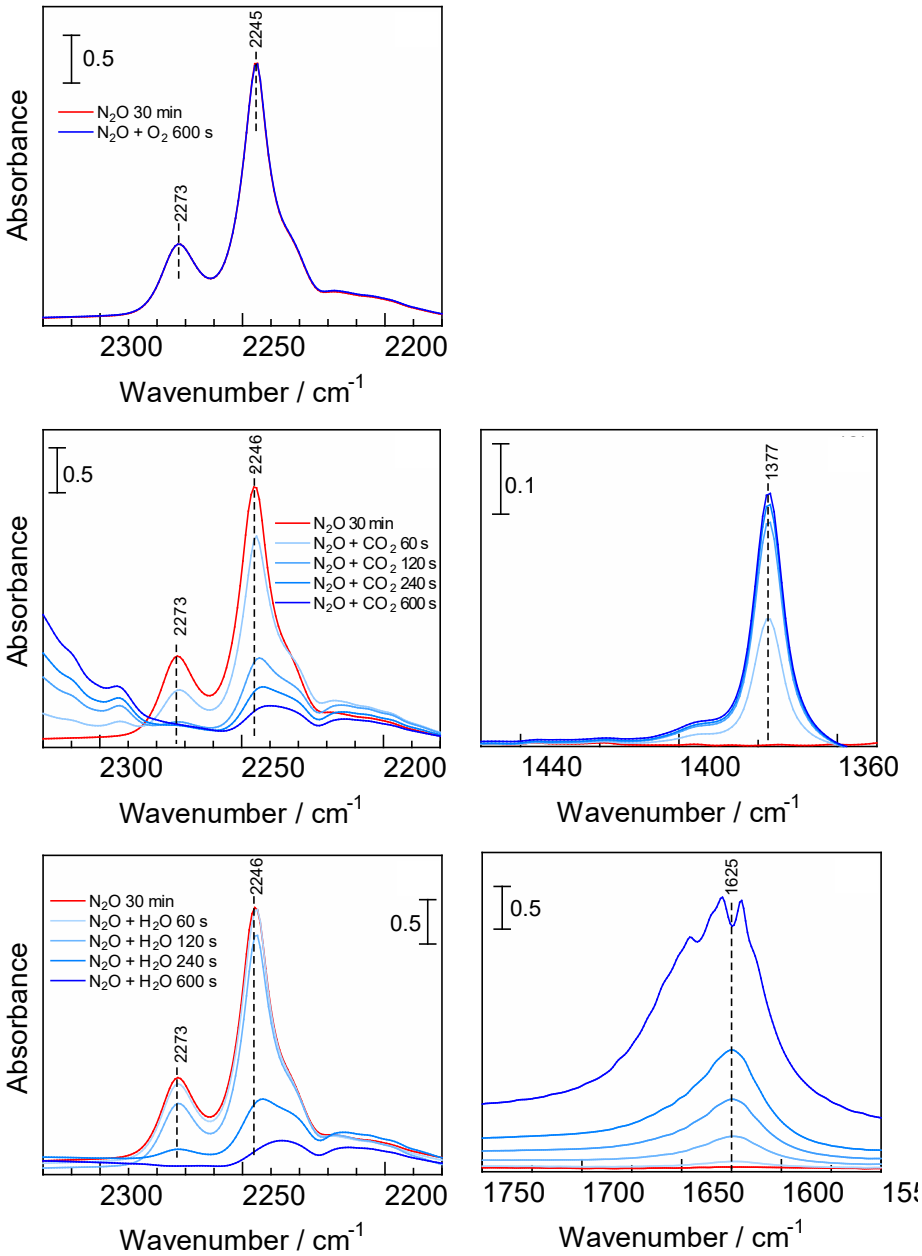

Figure 6. *In situ* IR spectra of Ca-MOR after the introduction of (A) 10% O_2, (B) 5% CO_2, and (C) 3% H_2O following the introduction of 0.1% N_2O at 50 °C for 30 min. Weight of Ca/MOR: 40mg, total flow rate: 50 mL/min. Before the introduction of 0.1% N_2O, the Ca-MOR pellet was pretreated under the flow of He at 500 °C for 30 min and then cooled to 50 °C.

https://doi.org/10.26434/chemrxiv-2024-0q1cm **ORCID:** https://orcid.org/0000-0002-6100-8247 Content not peer-reviewed by ChemRxiv. **License:** CC BY-NC 4.0

N_2O adsorption and reduction

Although N_2O is considered a significant greenhouse gas, its removal from gas streams remains challenging, especially at low temperatures and in the presence of O_2, which is prevalent in various N_2O sources.[47] In this study, we developed a continuous N_2O capture and reduction system in which N_2O could be selectively captured in the presence of O_2 and reduced to N_2 at relatively low temperatures, as shown in **Scheme 1**. Two reactors containing Ca-MOR were set up in parallel for the capture or release of N_2O. The effluent composition for N_2O capture was monitored by IR spectroscopy. After feeding 500 ppm N_2O + 10% O_2 for 40 min, the N_2O + O_2 feed was switched to the other reactor containing the same Ca-MOR material. The captured N_2O was released by heating the Ca-MOR to 150 °C at a heating rate of 20 °C/min, and then cooling to 50 °C. The liberated N_2O was fed into the downstream section of the system, where the $Pd/La/Al_2O_3$ catalyst was positioned and maintained at 150 °C throughout the process, along with a 4% H_2 flow. The composition of the effluent gas from the reactor equipped with $Pd/La/Al_2O_3$ was monitored using mass spectrometry.

Figure 7 shows the performance of the continuous N_2O capture and reduction system. During the heating of Ca-MOR from 50 to 150 °C, the formation of N_2 was observed with a maximum concentration of ~12000 ppm and almost no N_2O was detected, indicating that all the N_2O released from Ca-MOR was efficiently reduced into N_2 by H_2 over $Pd/La/Al_2O_3$. In addition, no N_2O was detected using IR (data not shown), indicating that almost all of the supplied N_2O was captured by Ca-MOR. These results reveal that the N_2O capture capacity and subsequent reduction ability of the continuous N_2O capture and reduction systems were preserved for at least 15 h (10 cycles) in the presence of O_2.

https://doi.org/10.26434/chemrxiv-2024-0q1cm **ORCID:** https://orcid.org/0000-0002-6100-8247 Content not peer-reviewed by ChemRxiv. **License:** CC BY-NC 4.0

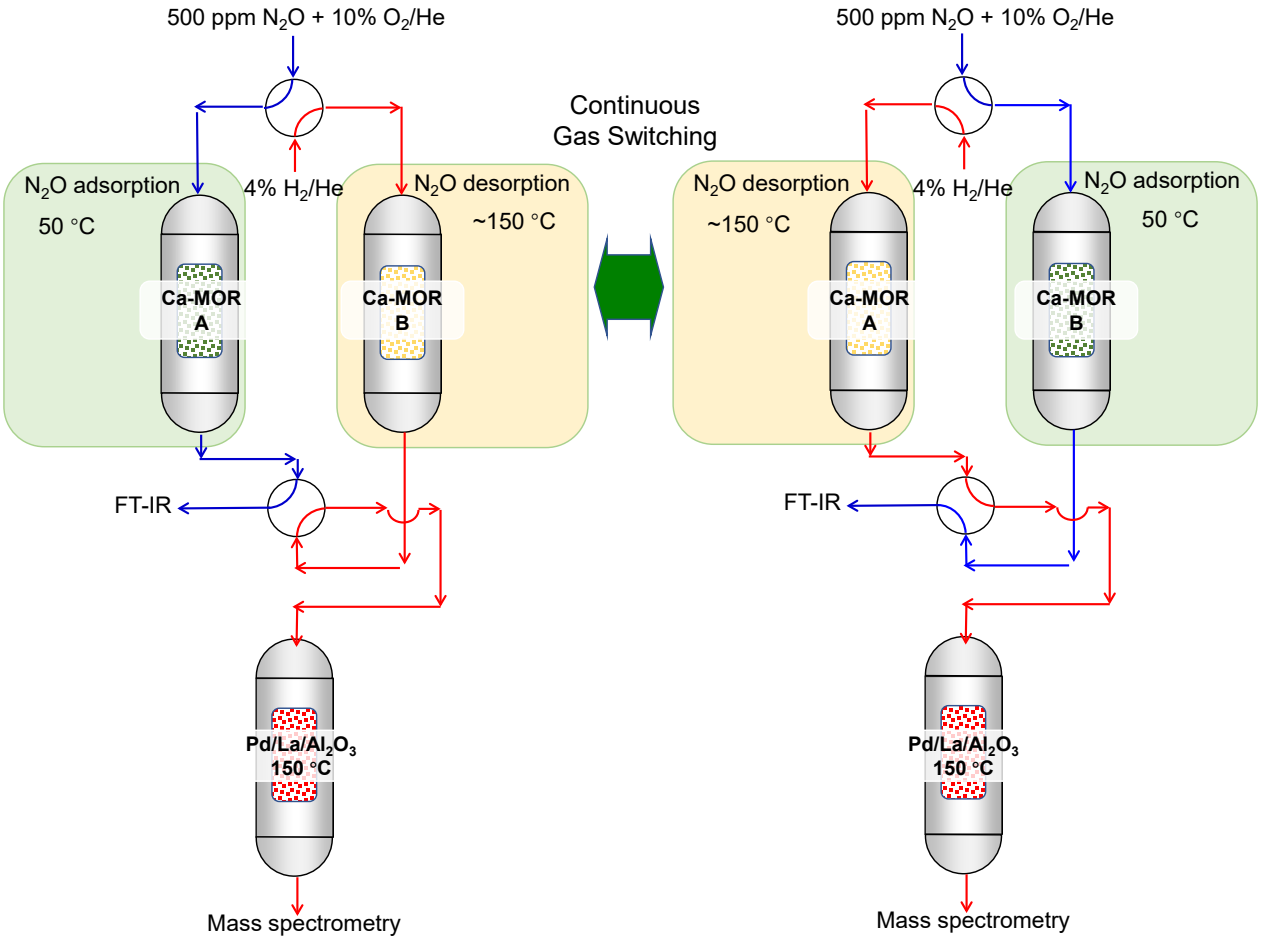

Scheme 1. Scheme of the continuous N_2O capture and reduction system using Ca-MOR zeolite as the N_2O capture adsorbent and Pd/La/Al_2O_3 as the reduction catalyst. The temperature of the Ca-MOR for N_2O capture was set to 50 °C, while the temperature was increased from 50 to 150 °C at a rate of 20 °C/min during the desorption phase. The downstream Pd/La/Al_2O_3 section was set at 150 °C throughout the process. The gas type was switched every 40 min.

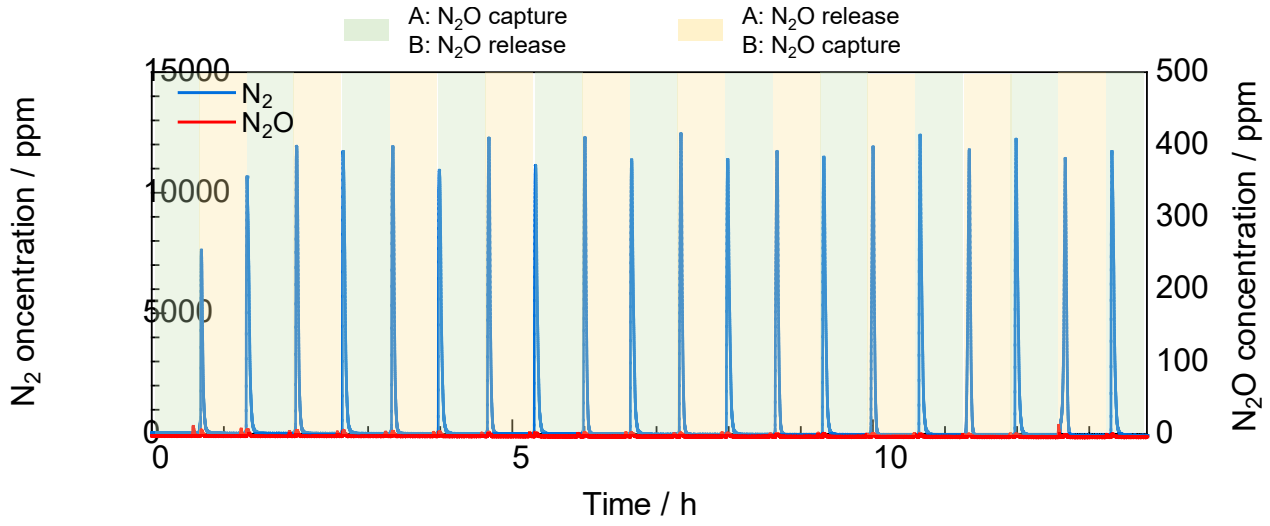

Figure 7. Performance of the Ca-MOR-Pd/La/Al_2O_3 continuous N_2O capture and reduction system. The gas fed to the Ca-MOR was switched between 500 ppm N_2O + 10% O_2 and 4% H_2/He every 40 min.

https://doi.org/10.26434/chemrxiv-2024-0q1cm **ORCID:** https://orcid.org/0000-0002-6100-8247 Content not peer-reviewed by ChemRxiv. **License:** CC BY-NC 4.0

Conclusions

In this study, a series of alkali metal-exchanged zeolite samples were prepared, and their N_2O capture capacities were estimated. The obtained results demonstrate that Ca-MOR shows high efficiency for N_2O capture. Therefore, a continuous N_2O capture and reduction system was developed using Ca-MOR as an N_2O adsorbent and $Pd/La/Al_2O_3$ for N_2O reduction. This process is suitable for continuous operation under temperature-swing cycles between 50 and 150 °C, and the N_2O capture and subsequent reduction performance was preserved for at least 15 h (10 cycles). Notably, this process can operate at low temperatures (below 150 °C) through a simple temperature-swing operation in the presence of O_2.

Experimental Section

Material preparation

Various zeolites were used to prepare the ion-exchanged zeolite materials: MOR (JRC-Z-HM20(5), Si/Al = 9.1, Tosoh Co.), MFI (HSZ-820NHA, Si/Al = 11.15, Tosoh Co.), CHA (Si/Al ratio = 11.15, Tosoh Co.), BEA (HSZ-920NHA, Si/Al = 8.75, Tosoh Co.), Y (HSZ-372HUA, Si/Al = 15, Tosoh Co.). The following compounds were used for zeolite ion exchange: $Mg(NO_3)_2$ (>99.2%, Kanto Chemical Co. Inc.), $Ca(NO_3)_2$ (>98.5%, Wako Pure Chemical Industries), $Sr(NO_3)_2$ (>98.0%, Kanto Chemical Co. Inc.), $Ba(NO_3)_2$ (>99.0%; Wako Pure Chemical Industries), $Ce(NO_3)_3$ (>98.0%; Wako Pure Chemical Industries). For ion exchange, 1 g of zeolite powder was mixed with 50 mL of an aqueous solution of the precursor in which the molar amount of the precursor was five times that of Al in the zeolite. The slurry was then heated at 60 °C for 4 h under strirring. The as-prepared sample was recovered by centrifugation at 4000 rpm, dried at 110 °C for 12 h, and then calcined at 500 °C for 3 h to obtain ion-exchanged zeolite materials. The La-containing Al_2O_3-supported Pd catalyst ($Pd/La/Al_2O_3$) was prepared using the impregnation method described in our previous paper.[48]

Characterization

X-ray diffraction (XRD) patterns were obtained using a Rigaku MiniFlex II/AP diffractometer with Cu-Kα radiation. The quantity of the incorporated metal species was determined using energy-dispersive X-ray fluorescence spectrometry (EDX-700HS, Shimadzu).

In situ infrared (IR) spectra were collected in transmission mode using an FT/IR-4600 (JASCO) unit with a TGS detector. A self-supporting disk of the sample (40 mg) was placed in a handmade *in situ* glass cell with CaF_2 windows. For *in situ* IR experiments, N_2O was fed into the cell at 50 °C through a conventional flow reaction system at a total flow rate of 100 mL/min. Before the measurements, the catalysts were pretreated *in situ* under He flow at 500 °C for 30 min. Temperature-programmed desorption of N_2O (N_2O-TPD) was performed using a BELCAT II instrument (MicrotracBEL). After the He pretreatmentat 500 °C for 30 min, the sample was exposed to 10%

https://doi.org/10.26434/chemrxiv-2024-0q1cm ORCID: https://orcid.org/0000-0002-6100-8247 Content not peer-reviewed by ChemRxiv. License: CC BY-NC 4.0

N_2O/He (20 mL/min) at 50 °C for 30 min, followed by purging with He for 10 min. The sample was heated to 250 °C at a rate of 10 °C/min.

Breakthrough experiments

Breakthrough experiments were performed with a feed of 500 ppm N_2O, 500 ppm N_2O + 5% CO_2, or 500 ppm N_2O + 3% H_2O at a total flow rate of 50 mL/min. Before the breakthrough experiment, the sample was pretreated under He flow (50 mL/min) at 500 °C for 30 min. The effluent gas stream was monitored using an online FT-IR spectrometer (JASCO FT/IR-4600) with a TGS detector (20 scans with a resolution of 4 cm^{-1}) and a custom-built gas cell (CaF_2 windows).

N_2O capture and reduction

N_2O capture and reduction experiments were performed using a continuously separated fixed-bed flow system (**Scheme 1**). Two reactors containing 300 mg of Ca-MOR zeolite were set in parallel, where one reactor captured the N_2O selectively from the mixture of 0.1% N_2O and 10% O_2 (50 mL/min, He balance), and the other released N_2O by heating the Ca-MOR zeolite from 50 to 150 °C (20 °C/min) under a flow of 4% H_2/He (50 mL/min). The effluent from the N_2O capture reactor was monitored using an online FT-IR spectrometer (JASCO FT/IR-4600) equipped with a TGS detector (20 scans at a resolution of 4 cm^{-1}). The released N_2O was then fed into a Pd/La/Al_2O_3 catalyst for the reduction of N_2O at 150 °C. The effluent of Pd/La/Al_2O_3 was monitored using a mass spectrometer (MS) apparatus (BELMass, MicrotracBEL Corp).

Computational methods

Periodic DFT calculations were performed using the Vienna Ab Initio Simulation Package (VASP, version 5.4.4)[38,39] and Matlantis.[40] For VASP, the Perdew–Burke–Ernzerhof functional revised for solids (PBEsol)[49] was employed in combination with the projector-augmented wave (PAW) method.[50] A kinetic energy cutoff of 400 eV was used for plane-wave basis sets. Gaussian smearing (width: 0.2 eV) was applied to occupy the electronic level. The k-point mesh included only the gamma point of the Brillouin zone (1 × 1 × 1). The van der Waals interactions are described using a dispersion-corrected DFT-D3 (BJ) function.[51] The convergence of the force on each atom was set to 0.03 eV $Å^{-1}$. The adsorption energy (E_{ads}) of a molecule is defined as:

$$E_{ads} = E_{A/S} - E_A - E_S \quad (1)$$

where $E_{A/S}$, E_A, and E_S are the electronic energies of the adsorption complex, free-state adsorbate, and the bare Ca-MOR structure, respectively.

Periodic universal neural network potential (NNP) calculations were performed using Matlantis (version 3.0.0, CRYSTAL_U0_PLUS_D3 mode: crystal systems (without Hubbard U correction) +

https://doi.org/10.26434/chemrxiv-2024-0q1cm ORCID: https://orcid.org/0000-0002-6100-8247 Content not peer-reviewed by ChemRxiv. License: CC BY-NC 4.0

DFT-D3 dispersion correction). All-atom energy optimizations were conducted using the Broyden–Fletcher–Goldfarb–Shanno algorithm with a force threshold of 0.01 eV $Å^{-1}$.

Ab initio thermodynamic analyses

Ab initio thermodynamic analysis[52,53] was performed to investigate the effects of the reaction gases (O_2 and H_2O) and temperature on the calcium oxide species in the alumina-loaded zeolites. The enthalpy and entropy at each temperature and standard state pressure (1 atm) were obtained from the NIST-JANAF Thermochemical Tables.[54] The energies of the gas molecules were obtained using a large empty unit cell (25 Å × 25 Å × 25 Å) to mimic the isolated species. The equilibrium reaction, energy change (ΔE), Gibbs free energy change (ΔG), and chemical potential change ($\Delta\mu$) under O_2 and H_2O atmospheres are given by Eqs. (2)–(5), respectively.

$$xCaO + SiO_2(Al) + \frac{1}{2}H_2O + \left(-\frac{1}{2}x + \frac{1}{2}y - \frac{1}{4}z\right)O_2 \rightarrow Ca_xO_yH_z/SiO_2(Al) \quad (2)$$

$$\Delta E = E\left[Ca_xO_yH_z/SiO_2(Al)\right] - xE[\mathrm{CaO}] - E[SiO_2(Al)] - \frac{1}{2}E[H_2O] - \left(-\frac{1}{2}x + \frac{1}{2}y - \frac{1}{4}z\right)E[O_2] \quad (3)$$

$$\Delta G(T,p) = \Delta E - \frac{1}{2}\Delta\mu_{H_2O} - \left(-\frac{1}{2}x + \frac{1}{2}y - \frac{1}{4}z\right)\Delta\mu_{O_2} \qquad \left(p = \frac{p_{gas}}{p^0}\right) \quad (4)$$

$$\Delta\mu_{gas} = \Delta\mu_{gas}(T,p^0) + RTln\left(\frac{p_{gas}}{p^0}\right) \ (\mathrm{gas} = \mathrm{O_2 \ and \ H_2O}) \quad (5)$$

Here, $Ca_xO_yH_z/SiO_2$(Al) is the Al-loaded Ca-MOR species, E[$Ca_xO_yH_z/SiO_2$(Al)] is the total energy of the species, E[SiO_2(Al)] is the total energy of the Al-loaded MOR model, E[O_2] and E[H_2O] are the total energies of the gas molecules, $\Delta\mu_{gas}$ is the change in the chemical potential of the gases involved in the reaction (Eq. (5)), T is the temperature (K), p^0 is the atmospheric pressure, and p_{gas} is the partial pressure of the reaction gas.

AUTHOR INFORMATION

Corresponding authors:
Yuan Jing, E-mail: jing.y.ab@m.titech.ac.jp
Ken-ichi Shimizu, E-mail : kshimizu@cat.hokudai.ac.jp
Takashi Toyao, E-mail : toyao@cat.hokudai.ac.jp

ACKNOWLEDGEMENTS

This study was financially supported by KAKENHI (Grant No. 20H02775, 20KK0111, 21H04626, and 22K14538) from the Japan Society for the Promotion of Science (JSPS) and by the Japanese Ministry of Education, Culture, Sports, Science, and Technology (MEXT) within the project “Integrated

https://doi.org/10.26434/chemrxiv-2024-0q1cm ORCID: https://orcid.org/0000-0002-6100-8247 Content not peer-reviewed by ChemRxiv. License: CC BY-NC 4.0

Research Consortium on Chemical Sciences (IRCCS).” All DFT calculations using VASP were performed using supercomputers at RIIT (Kyushu University) and ACCMS (Kyoto University).

Supporting Information

Additional data are given in the Supporting Information.

Keywords: N_2O decomposition, greenhouse gas, continuous capture and reduction, Ca-zeolite

https://doi.org/10.26434/chemrxiv-2024-0q1cm **ORCID:** https://orcid.org/0000-0002-6100-8247 Content not peer-reviewed by ChemRxiv. **License:** CC BY-NC 4.0

References

[1] A. R. Ravishankara, J. S. Daniel, R. W. Portmann, *Science (1979)* **2009**, *326*, 123–125.

[2] L. Li, J. Xu, J. Hu, J. Han, *Environ Sci Technol* **2014**, *48*, 5290–5297.

[3] K. Yamashita, Z. Liu, K. Iyoki, C. T. Chen, S. Miyagi, Y. Yanaba, Y. Yamauchi, T. Okubo, T. Wakihara, *Chem. Commun.* **2021**, *57*, 1312–1315.

[4] J. Pérez-Ramírez, F. Kapteijn, K. Schöffel, J. A. Moulijn, *Appl Catal B* **2003**, *44*, 117–151.

[5] M. Konsolakis, *ACS Catal* **2015**, *5*, 6397–6421.

[6] F. Kapteijn, J. Rodriguez-Mirasol, J. A. Moulijn, *Appl Catal B* **1996**, *9*, 25–64.

[7] A. Kudo, A. Mine, *Appl Surf Sci* **1997**, *121/122*, 538–542.

[8] M. Jabłońska, R. Palkovits, *Catal. Sci. Technol.* **2016**, *6*, 49–72.

[9] M. Jabłońska, M. A. Arán, A. M. Beale, G. Delahay, C. Petitto, M. Nocuń, R. Palkovits, *Appl Catal B* **2019**, *243*, 66–75.

[10] B. H. Ko, B. Hasa, H. Shin, Y. Zhao, F. Jiao, *J Am Chem Soc* **2022**, *144*, 1258–1266.

[11] K. Kim, J. Byun, H. Kim, K. S. Lee, H. S. Lee, J. Kim, T. Hyeon, J. J. Kim, J. W. Han, *ACS Catal* **2021**, *11*, 15089–15097.

[12] V. M. G. M. L. Ovcharov, *Theor. Exp. Chem.* **2021**, *57*, 30–63.

[13] J. Oi, A. Obuchi, G. R. Bamwenda, A. Ogata, H. Yagita, S. Kushiyama, K. Mizuno, *Appl Catal B* **1997**, *12*, 277–286.

[14] A. Satsuma, H. Maeshima, K. Watanabe, K. Suzuki, T. Hattori, *Catal Today* **2000**, *63*, 347–353.

[15] S. Parres-Esclapez, F. E. López-Suárez, A. Bueno-López, M. J. Illán-Gómez, B. Ura, J. Trawczynski, *Top Catal* **2009**, *52*, 1832–1836.

[16] M. J. Kim, Y. J. Kim, S. J. Lee, I. S. Ryu, H. J. Kim, Y. Kim, C. H. Ko, S. G. Jeon, *Chem. Eng. Res. Des.* **2019**, *141*, 455–463.

[17] Y. Li, A. Sundermann, O. Gerlach, K. Bin Low, C. C. Zhang, X. Zheng, H. Zhu, S. Axnanda, *Catal Today* **2020**, *355*, 608–619.

[18] S. Hinokuma, T. Iwasa, Y. Kon, T. Taketsugu, K. Sato, *Sci Rep* **2020**, *10*, DOI 10.1038/s41598-020-78744-x.

[19] S. Hinokuma, T. Iwasa, Y. Kon, T. Taketsugu, K. Sato, *Catal Commun* **2021**, *149*, DOI 10.1016/j.catcom.2020.106208.

[20] Y. Jing, K. Taketoshi, N. Zhang, C. He, T. Toyao, Z. Maeno, T. Ohori, N. Ishikawa, K. Shimizu, *ACS Catal* **2022**, *12*, 6325–6333.

[21] Y. Jing, C. He, N. Zhang, Y. Murano, R. Toyoshima, H. Kondoh, Y. Kageyama, H. Inomata, T. Toyao, K. Shimizu, *ACS Catal* **2023**, *13*, 12983–12993.

[22] M. Mauvezin, G. Delahay, B. Coq, S. Kieger, *Appl. Catal. B.* **1999**, *23*, L79–L82.

[23] G. Centi, S. Perathoner, F. Vazzana, M. Marella, M. Tomaselli, M. Mantegazza, *Adv Environ Res* **2000**, *4*, 325–338.

[24] X. Zhang, Q. Shen, C. He, C. Ma, J. Cheng, L. Li, Z. Hao, *ACS Catal* **2012**, *2*, 512–520.

https://doi.org/10.26434/chemrxiv-2024-0q1cm **ORCID:** https://orcid.org/0000-0002-6100-8247 Content not peer-reviewed by ChemRxiv. **License:** CC BY-NC 4.0

[25] A. Wang, Y. Wang, E. D. Walter, R. K. Kukkadapu, Y. Guo, G. Lu, R. S. Weber, Y. Wang, C. H. F. Peden, F. Gao, *J Catal* **2018**, *358*, 199–210.

[26] M. C. Campa, D. Pietrogiacomi, C. Scarfiello, L. R. Carbone, M. Occhiuzzi, *Appl Catal B* **2019**, *240*, 367–372.

[27] Y. You, S. Chen, J. Li, J. Zeng, H. Chang, L. Ma, J. Li, *J Hazard Mater* **2020**, *383*, 121117.

[28] J. Cheng, D. Zheng, G. Yu, R. Xu, C. Dai, N. Liu, N. Wang, B. Chen, *ACS Catal* **2023**, *13*, 934–947.

[29] S. Kar, A. Goeppert, G. K. S. Prakash, *Acc Chem Res* **2019**, *52*, 2892–2903.

[30] M. González-Castaño, B. Dorneanu, H. Arellano-García, *React Chem Eng* **2021**, *6*, 954–976.

[31] F. Kosaka, Y. Liu, S. Y. Chen, T. Mochizuki, H. Takagi, A. Urakawa, K. Kuramoto, *ACS Sustain Chem Eng* **2021**, *9*, 3452–3463.

[32] L. Li, Z. Wu, S. Miyazaki, T. Toyao, Z. Maeno, K. Shimizu, *RSC Adv* **2023**, *13*, 2213–2219.

[33] L. Li, S. Miyazaki, Z. Wu, T. Toyao, R. Selyanchyn, Z. Maeno, S. Fujikawa, K. Shimizu, *Appl Catal B* **2023**, *339*, 123151.

[34] M. Brandle, J. Sauer, *J Am Chem Soc* **1998**, *120*, 1556–1570.

[35] R. Grybos, J. Hafner, L. Benco, P. Raybaud, *J. Phys. Chem. C* **2008**, *112*, 12349–12362.

[36] S. Grundner, M. A. C. Markovits, G. Li, M. Tromp, E. A. Pidko, E. J. M. Hensen, A. Jentys, M. Sanchez-Sanchez, J. A. Lercher, *Nat Commun* **2015**, *6*, 7546.

[37] H. Xia, *ACS Omega* **2020**, *5*, 9707–9713.

[38] G. Kresse, J. Furthmüller, *Phys Rev B* **1996**, *54*, 11169.

[39] G. Kresse, J. Furthmüller, *Comput Mater Sci* **1996**, *6*, 15–50.

[40] S. Takamoto, C. Shinagawa, D. Motoki, K. Nakago, W. Li, I. Kurata, T. Watanabe, Y. Yayama, H. Iriguchi, Y. Asano, T. Onodera, T. Ishii, T. Kudo, H. Ono, R. Sawada, R. Ishitani, M. Ong, T. Yamaguchi, T. Kataoka, A. Hayashi, N. Charoenphakdee, T. Ibuka, *Nat Commun* **2022**, *13*, 2991.

[41] T. M. Miller, V. H. Grassian, *J. Am. Chem. Soc* **1995**, *117*, 10969–10975.

[42] D. Pietrogiacomi, M. C. Campa, L. R. Carbone, S. Tuti, M. Occhiuzzi, *Appl Catal B* **2016**, *187*, 218–227.

[43] B. Yue, X. Lian, S. Liu, G. Wu, J. Xu, L. Li, *Chemical Engineering Journal* **2023**, *462*, 142300.

[44] L. Wang, J. Liu, C. Lin, H. Shang, J. Yang, L. Li, J. Li, *Chemical Engineering Journal* **2022**, *431*, 134257.

[45] E. Meloni, M. Martino, M. Pierro, P. Pullumbi, F. Brandani, V. Palma, *Energies (Basel)* **2022**, *15*, 4119.

[46] L. Ohlin, V. Berezovsky, S. Öberg, A. Farzaneh, A. Holmgren, M. Grahn, *J. Phys. Chem. C* **2016**, *120*, 29144–29152.

[47] H. Tian, R. Xu, J. G. Canadell, R. L. Thompson, W. Winiwarter, P. Suntharalingam, E. A. Davidson, P. Ciais, R. B. Jackson, G. Janssens-Maenhout, M. J. Prather, P. Regnier, N. Pan, S. Pan, G. P. Peters, H. Shi, F. N. Tubiello, S. Zaehle, F. Zhou, A. Arneth, G. Battaglia, S. Berthet, L. Bopp, A. F. Bouwman, E. T. Buitenhuis, J. Chang, M. P. Chipperfield, S. R. S. Dangal, E. Dlugokencky, J. W. Elkins, B. D. Eyre, B. Fu, B. Hall, A. Ito, F. Joos, P. B. Krummel, A. Landolfi, G. G. Laruelle, R. Lauerwald, W. Li, S. Lienert, T. Maavara, M. MacLeod, D. B. Millet, S. Olin, P. K. Patra, R. G. Prinn, P. A. Raymond, D. J. Ruiz, G. R. van der Werf, N. Vuichard, J. Wang, R. F. Weiss, K. C. Wells, C. Wilson, J. Yang, Y. Yao, *Nature* **2020**, *586*, 248–256.

[48] Y. Jing, Z. Cai, C. Liu, T. Toyao, Z. Maeno, H. Asakura, S. Hiwasa, S. Nagaoka, H. Kondoh, K. Shimizu, *ACS Catal* **2020**, *10*, 1010–1023.

https://doi.org/10.26434/chemrxiv-2024-0q1cm **ORCID:** https://orcid.org/0000-0002-6100-8247 Content not peer-reviewed by ChemRxiv. **License:** CC BY-NC 4.0

[49] J. P. Perdew, A. Ruzsinszky, G. I. Csonka, O. A. Vydrov, G. E. Scuseria, L. A. Constantin, X. Zhou, K. Burke, *Phys Rev Lett* **2008**, *100*, 136406.

[50] P. E. Blöchl, *Phys Rev B* **1994**, *50*, 17953.

[51] S. Grimme, S. Ehrlich, L. Goerigk, *J Comput Chem* **2011**, *32*, 1456–1465.

[52] J. Rogal, K. Reuter, *Educational Notes RTO-EN-AVT-142* **2007**, *2*, 1–18.

[53] S. Yasumura, H. Ide, T. Ueda, Y. Jing, C. Liu, K. Kon, T. Toyao, Z. Maeno, K. Shimizu, *JACS Au* **2021**, *1*, 201–211.

[54] M. W. CHASE, *NIST-JANAF Thermochemical Tables.*, American Chemical Society, Washington, DC, **1998**.

https://doi.org/10.26434/chemrxiv-2024-0q1cm **ORCID:** https://orcid.org/0000-0002-6100-8247 Content not peer-reviewed by ChemRxiv. **License:** CC BY-NC 4.0

Entry for the Table of Contents

FULL PAPER

A two-step system for capturing and reducing N_2O has been developed, utilizing CaO-incorporated zeolites (Ca-zeolites) as an N_2O adsorbent and Pd nanoparticles supported on La-containing Al_2O_3 ($Pd/La/Al_2O_3$) as a reduction catalyst. This process is designed for continuous operation within a temperature range of 50–150 °C. The N_2O capture capacity and subsequent reduction ability of the system was maintained for at least 15 h (10 cycles). Notably, this process can operate at low temperatures (below 150 °C) via a simple temperature-swing process in the presence of O_2.

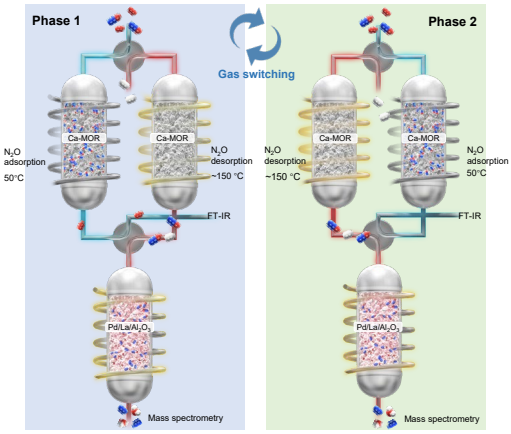

Yuan Jing*, Chenxi He, Li Wan, Jiahuan Tong, Jialei Zhang, Shinya Mine, Ningqiang Zhang, Yuuta Kageyama, Hironori Inomata, Ken-ichi Shimizu*, and Takashi Toyao*

Page No. – Page No.

Continuous N_2O capture and reduction to N_2 using Ca-zeolite absorbent and $Pd/La/Al_2O_3$ reduction catalyst

https://doi.org/10.26434/chemrxiv-2024-0q1cm **ORCID:** https://orcid.org/0000-0002-6100-8247 Content not peer-reviewed by ChemRxiv. **License:** CC BY-NC 4.0